Journal of Coordination Chemistry
Publication details, including instructions for authors and subscription information:
http://www.tandfonline.com/loi/gcoo20

pH-Controlled syntheses of two hybrids based on octamolybdate and enrofloxacin

Jingquan Sha [a], Yuhong Zhang [a], Liye Liang [a], Hongbin Qiu [a] & Mingyuan Liu [a]

[a] The Provincial Key Laboratory of Biological Medicine Formulation, School of Pharmacy, Jiamusi University, Jiamusi 154007, P.R. China

Accepted author version posted online: 18 Jul 2012.Published online: 02 Aug 2012.

To cite this article: Jingquan Sha, Yuhong Zhang, Liye Liang, Hongbin Qiu & Mingyuan Liu (2012) pH-Controlled syntheses of two hybrids based on octamolybdate and enrofloxacin, Journal of Coordination Chemistry, 65:18, 3264-3273, DOI: 10.1080/00958972.2012.713101

To link to this article: http://dx.doi.org/10.1080/00958972.2012.713101

Journal of Coordination Chemistry
Vol. 65, No. 18, 20 September 2012, 3264–3273

pH-Controlled syntheses of two hybrids based on octamolybdate and enrofloxacin

JINGQUAN SHA*, YUHONG ZHANG, LIYE LIANG, HONGBIN QIU and MINGYUAN LIU

The Provincial Key Laboratory of Biological Medicine Formulation, School of Pharmacy, Jiamusi University, Jiamusi 154007, P.R. China

(*Received 23 April 2012; in final form 12 June 2012*)

Two new drug molecules modifying octamolybdate-based hybrid compounds, $H_2[Ni(L)_2(H_2O)_2]\cdot(\beta\text{-}Mo_8O_{26})\cdot H_2O$ (**1**) and $[Ni_2L_2(H_2O)_4(\alpha\text{-}Mo_8O_{26})]$ (**2**) (L = enrofloxacin), have been synthesized at different pH values under hydrothermal conditions. Compound **1** was synthesized at pH ≈ 5, in which the octamolybdate shows β-isomer and the isolated Ni-enrofloxacin coordination subunits array on both sides of $\beta\text{-}Mo_8O_{26}$. Compound **2** was synthesized at pH ≈ 4, with octamolybdate showing the α-isomer and Ni-enrofloxacin having 1-D chain structure along the *a*-axis with $\alpha\text{-}Mo_8$ polyoxoanions connecting adjacent Ni1 along the *c*-axis generating another 1-D inorganic chain. As a result, the two kinds of 1-D chains cross each other forming a 2-D layer structure. The structures of **1** and **2** reveal that pH of the reaction system plays a crucial role in assembly of octamolybdate-based hybrid compounds. Investigation of the antitumor activities on SGC7901 and SMMC7721 cells of **1** and **2** indicates that the two new compounds possess selective antitumor activities, and their antitumor activities can be modulated by transition metal complexes.

Keywords: Polyoxometalates; Octamolybdates; Enrofloxacin; Antitumor activity

1. Introduction

Organic–inorganic hybrid multifunctional compounds have been an area of rapid growth. Polyoxometalates (POMs), a diverse ensemble of nanostructures with an almost infinite variability of chemical, physical, and biological properties, have also attracted attention [1–3]. An intriguing area is the development of inorganic–organic hybrids consisting of POMs and ligands for medical applications. This field is in its infancy, but first approaches are reported, such as amino acid-functionalized POMs [4], fluorouracil-containing $[BW_{12}O_{40}]^{5-}$ [5], surfactant and dendritic encapsulated clusters, as well as starch and liposome encapsulated POMs [6].

The main problems preventing application of POMs in medicine were low hydrolytic stability and, in particular, low selectivity (accumulation in the

*Corresponding author. Email: shajq2002@126.com

Journal of Coordination Chemistry
ISSN 0095-8972 print/ISSN 1029-0389 online
http://dx.doi.org/10.1080/00958972.2012.713101

reticuloendothelial system). Additionally, toxicity of POMs is strongly dependent on the structure, comprising low-toxic POMs ($[SiW_{12}O_{40}]^{4-}$, $[PW_{12}O_{40}]^{3-}$) and high-toxic compounds, such as HPA-23 [7]. To solve these problems, modifying of POMs is a promising route [8, 9], as nearly every molecular property that impacts recognition and reactivity of POMs with target biological macromolecules can be easily altered, such as polarity, redox, surface charge distribution, shape, and acidity. Another is that the surface of POMs can be modified to enable design of multifunctional compounds by covalent attachment of organic groups. During our efforts to modify and functionalize POMs with biologically active molecules [10], quinolones capture our attention, because quinolones can act as antibacterial drugs and excellent multidentate ligands coordinating with metal ions. Structures of metal complexes of quinolones have been reported [11, 12], and the results suggest that metal ion coordination might be involved in antibacterial activity and improve drug activity. So enrofloxacin ($C_{19}H_{22}FN_3O_3$, 1-cyclopropyl-7-(4-ethyl-1-piperazine)-6fluoro-1,4-dihydro-4-oxy-3-quinoline carboxylic acid) (scheme 1), a typical second-generation quinolone antimicrobial drug [13] with a broad spectrum of activity against a wide range of Gram-negative and Gram-positive bacteria, was used.

Many POM-based hybrids have been synthesized; among them octamolybdate is an important branch because of their varied structural patterns in the solid state, including α-, β-, γ-, δ-, ε-, ζ-, and η-Mo_8O_{26} [14–17], which can transform in response to environmental restraints. These isomers not only provide a large number of terminal and bridging oxygen atoms as multidentate inorganic ligands, but also exhibit a variety of structural motifs with different sizes and topologies. As reported previously, pH of the reaction system is crucial for formation of the isomers [18, 19]. Here we report the syntheses, crystal structures, and antitumor activities of two organic–inorganic hybrids based on octamolybdate and enrofloxacin, $H_2[Ni(L)_2(H_2O)_2]\cdot(\beta\text{-}Mo_8O_{26})\cdot H_2O$ (**1**) and $[Ni_2L_2(H_2O)_4(\alpha\text{-}Mo_8O_{26})]$ (**2**). Their structures show that pH plays a key role during assembly. Investigation of the antitumor activities on SGC7901 and SMMC7721 cells of **1** and **2** indicates that introduction of Ni-enrofloxacin onto the polyoxoanion surface can modulate antitumor activity; the two new compounds possess selectivity in antitumor activities.

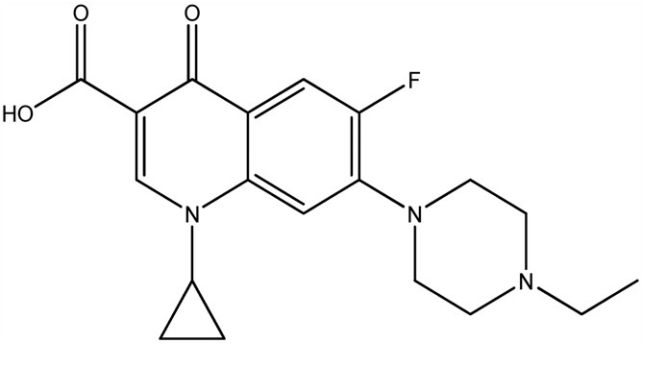

Scheme 1. The structure of enrofloxacin.

2. Experimental

2.1. *General procedures*

All reagents were purchased commercially and used without purification. Elemental analyses were performed on a Perkin-Elmer 2400 CHN Elemental Analyzer (C, H, and N) and a Leaman inductively coupled plasma spectrometer (Ni). IR spectra as KBr pellets were recorded on a Nicolet 170SX FT-IR spectrophotometer from 400 to 4000 cm^{-1}. TG analysis was performed on a Perkin-Elmer TGA7 instrument in flowing air with a heating rate of 10°C min^{-1}. XRPD patterns were obtained with a Rigaku D/max 2500V PC diffractometer with Cu-Kα radiation; the scanning rate is 4° s^{-1}, 2θ ranging from 5 to 50°.

2.2. *Syntheses*

2.2.1. $H_2[NiL_2(H_2O)_2]\cdot(\beta\text{-}Mo_8O_{26})\cdot H_2O$ (1). A mixture of $(NH_4)_6Mo_7O_{24}\cdot 4H_2O$ (0.2 g, 0.16 mmol), $NiSO_4\cdot 6H_2O$ (0.05 g, 0.2 mmol), enrofloxacin (0.07 g, 0.2 mmol), triethylamine (0.1 mmol), and H_2O (10 mL) was stirred at ambient temperature for 60 min and the pH adjusted to 5.0 with NaOH (1 mol L^{-1}) solution and then transferred and sealed in a 18 mL Teflon-lined stainless steel container, which was heated at 160°C for 96 h and then cooled to room temperature at 10°C h^{-1}. Green crystals of **1** were filtered and washed with distilled water (21% yield based on Mo). Anal. Calcd for $C_{38}H_{50}NiF_2N_6Mo_8O_{35}$ (2015) (%): C, 22.63; H, 2.48; N, 4.16; Ni, 2.91. Found (%): C, 22.60; H, 2.65; N, 4.15; Ni, 2.89.

2.2.2. $[Ni_2L_2(H_2O)_4(\alpha\text{-}Mo_8O_{26})]$ (2). The synthetic method here was similar to that used for the preparation of **1**, except that the pH was adjusted to 4.0. Green crystals of **2** were filtered and washed with distilled water (19% yield based on Mo). Anal. Calcd for $C_{38}H_{50}Ni_2F_2N_6Mo_8O_{36}$ (2089) (%): C, 21.82; H, 2.39; N, 4.02; Ni, 5.61. Found (%): C, 21.81; H, 2.55; N, 4.01; Ni, 5.58.

2.3. *X-ray crystallographic study*

Crystal data for **1** and **2** were collected on a Bruker SMART-CCD diffractometer with Mo-Kα monochromated radiation ($\lambda = 0.71073$ Å) at 293 K. Multiscan absorption corrections were applied. All the structures were solved by direct methods and refined by full-matrix least-squares on F^2 using the SHELXTL crystallographic software package [20]. The positions of hydrogen atoms on carbons were calculated theoretically. A summary of the crystal data, data collection, and refinement parameters for **1** and **2** are listed in table 1. Selected bond lengths and angles for **1** and **2** are listed in tables S1 and S2.

2.4. *Antitumor activity studies*

The antitumor activities of **1** and **2** and the β-Mo_8 cluster on the SGC7901 and SMMC7721 cells were tested by the MTT experiment. MTT is a dye, which can accept a

Table 1. Crystal data and structure refinements for **1** and **2**.

Compounds	**1**	**2**
Empirical formula	$C_{38}H_{52}NiF_2N_6Mo_8O_{35}$	$C_{38}H_{52}Ni_2F_2N_6Mo_8O_{36}$
Formula weight	2017	2091
Wavelength (Å)	0.71069	0.71069
Crystal system	Triclinic	Triclinic
Space group	$P\bar{1}$	$P\bar{1}$
Unit cell dimensions (Å, °)		
a	10.135(5)	10.5916(9)
b	11.944(6)	11.9709(10)
c	14.772(7)	12.0069(10)
α	98.122(6)	80.757(1)
β	109.854(6)	84.688(1)
γ	111.986(6)	79.057(1)
Volume (Å^3), Z	1483.9(13), 1	1472.3(2), 2
Calculated density (Mg m^{-3})	2.244	2.483
Absorption coefficient (mm^{-1})	2.048	2.377
F(000)	972	1010
Reflections collected	8773	8166
Independent reflection	6449 [R(int) = 0.0310]	5728 [R(int) = 0.0257]
Goodness-of-fit on F^2	1.405	1.012
Final R indices [$I > 2\sigma(I)$][a,b]	$R_1 = 0.0725$; $wR_2 = 0.2162$	$R_1 = 0.0426$; $wR_2 = 0.1208$
R indices (all data)[a,b]	$R_1 = 0.1027$; $wR_2 = 0.2396$	$R_1 = 0.0648$; $wR_2 = 0.1592$

[a] $R_1 = \sum||F_o| - |F_c||/\sum|F_o|$; [b] $wR_2 = \sum[w(F_o^2 - F_c^2)^2]/\sum[w(F_o^2)^2]^{1/2}$.

hydrogen atom. Surviving tumor cells are able to reduce the yellow MTT to an insoluble blue formazan in water whereas dead tumor cells do not possess this capability. The formazan product is dissolved in DMSO and then determined colorimetrically with a Microplate Reader (490 nm). Subcultured SGC7901 and SMMC7721 cells were suspended in 0.25% trypsin, respectively. The cell suspension (*ca* 10^5–10^6 cells mL) was added to a 96-well plate (100 µL per well) and incubated at 37°C in a 5% CO_2 incubator for 24 h. 100 µL samples containing the compounds were then added. After 72 h, 20 µL MTT solution (5 mg mL^{-1} in 0.01 mol L^{-1} phosphate buffer solution) was added, and the mixture was allowed to incubate for 4 h. The supernatant was removed and DMSO (150 µL) was added. The resulting mixture was shaken for 10 min at room temperature and colorimetric analysis was used to examine the cell survival rate. These samples containing **1** and **2** and the parent compound were obtained by dissolving in DMSO, autoclaving and diluting by an RPMI 1640 medium to a final concentration of 800, 400, 200, 100, 50, 25, 12.5, or 6.25 µg mL^{-1}.

3. Results and discussion

3.1. *Syntheses*

Although the syntheses of hybrids are sometimes quite complicated, and the relationship between reagents and the resulting compounds not always obvious, hydrothermal technique is an extremely convenient method for preparation of metastable hybrids. Several factors influence formation of crystal phases, such as

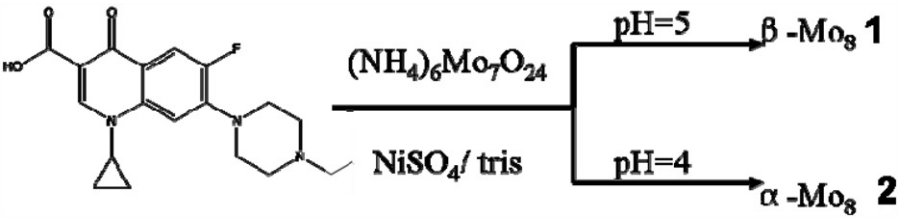

Scheme 2. Experimental conditions for the syntheses of **1** and **2**.

initial reactants, molar ratio, pH, reaction time, and temperature. Parallel experiments show that pH of the reaction system is crucial for formation of the compounds (scheme 2). Compounds **1** and **2** could only be obtained at pH of 5 for **1** and 4 for **2**, which shows pH-dependent competition in self-assembly of different products under hydrothermal conditions. Triethylamine is a universal reducer and mineralizer in the hydrothermal system and its presence is crucial to obtain **1** and **2**. Attempts to synthesize **1** and **2** without triethylamine produced floccules instead.

3.2. *Crystal structures*

3.2.1. Structure description of 1. Compound **1** is constructed from one $\{\beta\text{-}Mo_8O_{26}\}^{4-}$ cluster (shortened as β-Mo_8), an isolated Ni-enrofloxacin subunit $[Ni(L)_2(H_2O)_2]^{2+}$, and one lattice water molecule (figure 1a). The β-Mo_8 consists of a compact arrangement of eight edge-sharing $\{MoO_6\}$ octahedra shown in figure 1(b). Six molybdenum sites exhibit two terminal oxo-groups, while the central pair of molybdenum sites exhibits a single-terminal oxo-group. There are six μ2-, four μ3-, and two μ5-oxo-groups. Bond lengths and angles are in normal ranges. There is a crystallographically unique Ni, which exhibits octahedral configuration by four oxygen atoms from two enrofloxacin ligands (Ni1–O13 = 2.010 Å, Ni1–O14 = 2.023 Å) and two water moleucles (Ni1–O2W = 2.146 Å). Lattice waters O1W link adjacent β-Mo_8 clusters forming the 1-D POM-water chain shown in figure 1(c). There are extensive $\pi\cdots\pi$ interactions among organic ligands, which result in a 1-D supramolecular drug-metal hybrid chain constructed by adjacent Ni-enrofloxacin subunits, with centroid$\cdots$centroid distance between two adjacent aryl rings of 4.039 Å (figure 1c). These inorganic POM-water chains are connected by $[Ni(L)_2(H_2O)_2]^{2+}$ cations through bridging oxygen atoms and coordinated water, then form the 2-D supramolecular layer shown in figure 1(c). Finally, due to supramolecular interactions, including hydrogen bonds and π-stacking between 2-D layers in a parallel fashion, the 3-D architecture of **1** is stabilized (shown in figure S1).

3.2.2. Structure description of 2. Single-crystal X-ray diffraction analysis reveals that **2** is constructed by an α-Mo_8 cluster and an Ni-enrofloxacin coordination subunit $[Ni_2L_2(H_2O)_4]^{4+}$ shown in figure 2(a). The octamolybdate cluster in **2** is the α-isomer, which consists of six distorted $\{MoO_6\}$ octahedra and two distorted $\{MoO_4\}$ tetrahedra with three kinds of oxygen atoms (six μ_2-O, six μ_3-O, and fourteen O_t) (figure 2b).There are two crystallographically unique Ni^{II} cations, and each Ni^{II} cation exhibits

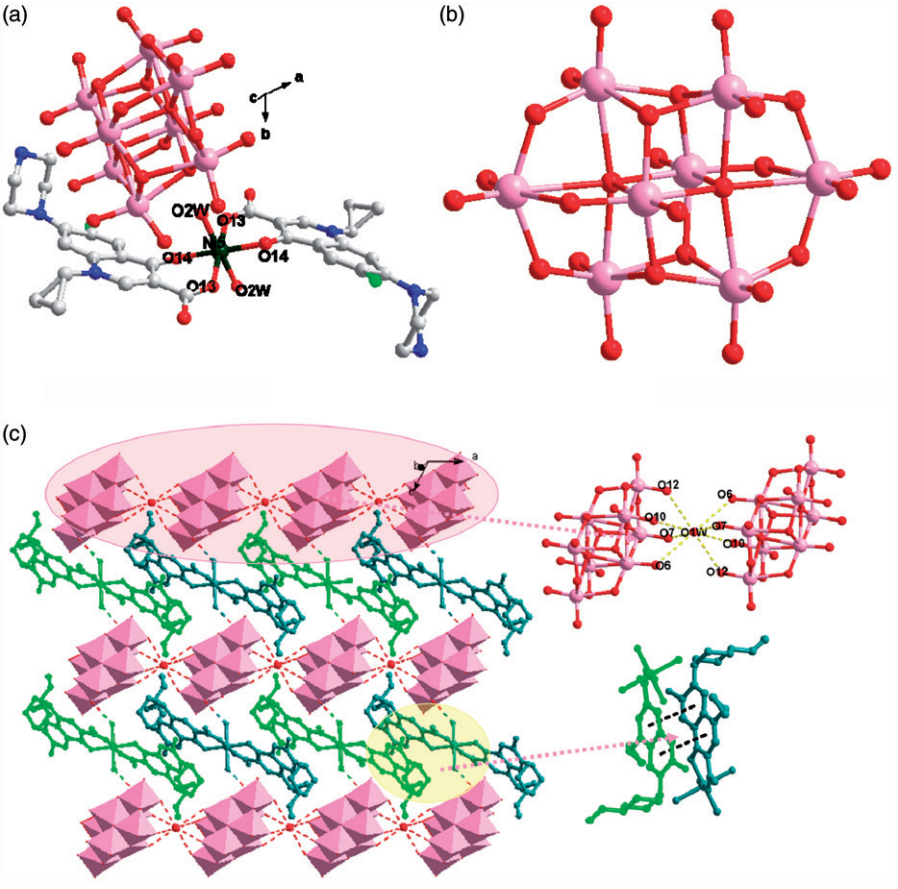

Figure 1. (a) Stick/polyhedral representation asymmetric unit of **1**. Only some atoms are labeled and lattice water molecules and hydrogen atoms are omitted for clarity. (b) Ball-stick representations of β-Mo_8 cluster. (c) 2-D layer structure formed by 1-D inorganic POM chains and 1-D organic drug chains.

octahedral geometry. Ni1 is six-coordinate by two oxygen atoms from two enrofloxacin ligands (Ni1–O6 = 2.065 Å), two terminal oxygen atoms from two α-Mo_8 anions (Ni1–O16 = 2.046 Å), and two water molecules (Ni1–O1W = 2.087 Å); Ni2 is also six-coordinate by two oxygen atoms of two water molecules (Ni2-O2W = 2.144 Å) and four oxygen atoms from two enrofloxacin ligands (Ni2–O15 = 2.021 Å, Ni2–O18 = 1.976 Å). The α-Mo_8 polyoxoanion as a bidentate inorganic ligand connects two adjacent Ni1 atoms generating a 1-D inorganic chain along the *c*-axis *via* two terminal oxygen atoms. Enrofloxacin as bridging linker connects adjacent Ni's generating a 1-D organic–inorganic chain along the *a*-axis. As a result, two kinds of 1-D chains cross each other, forming the 2-D layer structure (figure 2c). Finally, these layers form 3-D supramolecular structures through supramolecular interactions (figure S2).

3.3. *XRPD characterization, FT-IR spectra, and TG-DTA analysis*

The XRPD patterns for **1** and **2** are presented in figure S3. Diffraction peaks of both simulated and experimental patterns match well, indicating that the phase purities of **1**

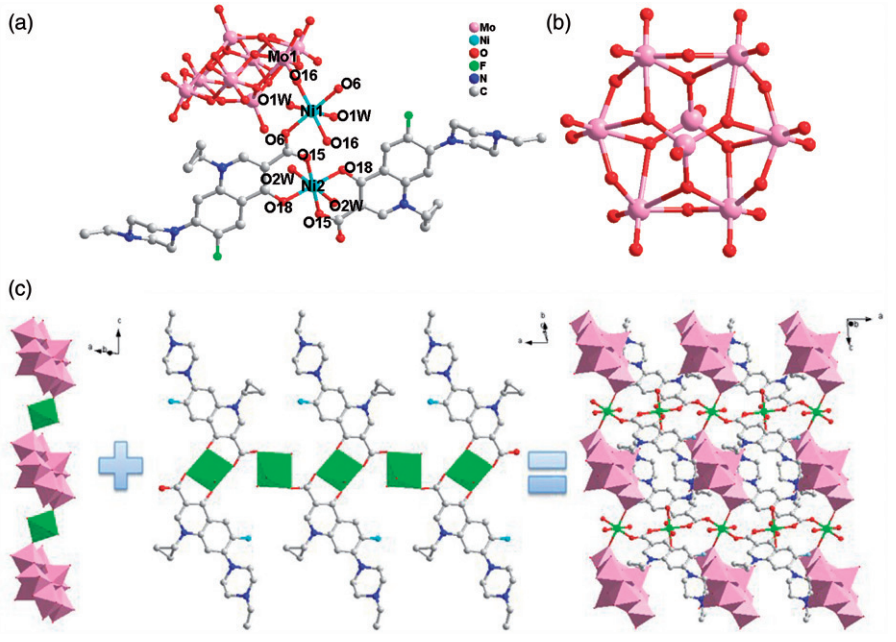

Figure 2. (a) Stick/polyhedral representation of the asymmetric unit of **2**. Only some atoms are labeled; lattice water molecules and hydrogen atoms are omitted for clarity. (b) Ball-stick representations of α-Mo_8 cluster. (c) 2-D layer structure formed by 1-D inorganic POM chains and 1-D organic drug chains.

and **2** are good. The difference in reflection intensities between the simulated and the experimental patterns is due to different orientation of the crystals in the powder samples. IR spectra for **1** and **2** are presented in figure S4 and figure S5, respectively. Bands at 1630–1030 cm^{-1} are associated with enrofloxacin [21]. Bands at 960–650 cm^{-1} are ascribed to ν(Mo = O) and ν(Mo–O–Mo) vibrations [18, 22]. Additionally, in order to characterize fully the thermal stabilities, their thermal behaviors were studied by TG-DTA (figure S6). The experiment was performed on crystalline samples under air. For **1**, thermal analysis gives a total loss of 40.13% from 30°C to 488°C, which agrees with the calculated weight loss of 40.05%; the first weight loss of 4.52% at 30–255°C corresponds to loss of five water molecules per formula (Calcd 4.46%) and the second continuous weight loss of 35.61% at 255–488°C arises from decomposition of enrofloxacin (Calcd 35.59%). Weight losses at 390°C and 415°C are followed by strong exothermic peaks in DTA curves, corresponding to decomposition of organic molecules. For **2**, thermal analysis is similar to that of **1** with first weight loss of 3.51% at 30–270°C from loss of four water molecules (Calcd 3.44%) and the second continuous weight loss of 34.42% at 270–470°C from decomposition of enrofloxacin (Calcd 34.34%). Weight losses at 393°C and 416°C are followed by strong exothermic peaks in DTA curves, corresponding to decomposition of organic molecules. These results further confirm the formulae of compounds.

3.4. *Antitumor activity studies*

A comparison of antitumor activities on SGC7901 and SMMC7721 cells for **1**, **2**, and β-Mo_8 was made (table S3). The inhibitory effect against SGC7901 cell lines shows that

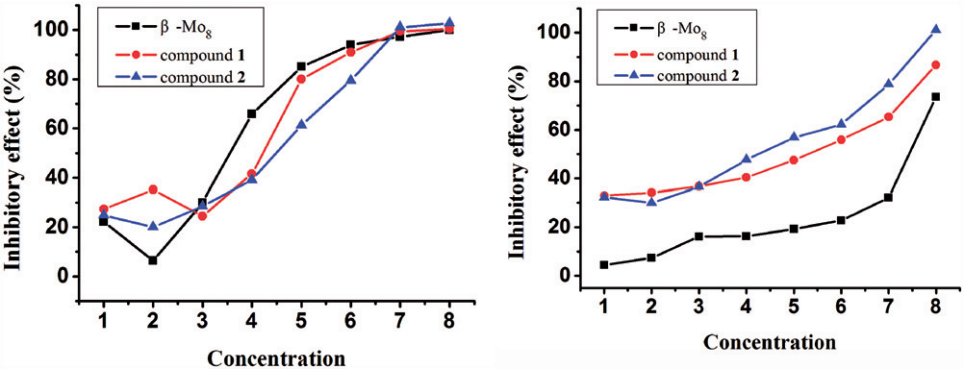

Figure 3. Curve of the anti-tumor activity against SGC7901 (left) and SMMC7721 (right) for **1** and **2** and the β-Mo_8 cluster (concentration: 1, 2, 3, 4, 5, 6, 7, and 8 represent 6.25, 12.5, 25, 50, 100, 200, 400, and 800 $\mu g\,mL^{-1}$, respectively).

1, **2**, and β-Mo_8 all exhibit high antitumor activities to SGC7901 (figure 3, left). The 50% lethal concentration (IC_{50}) against SGC7901 cells for β-Mo_8 and **1** and **2** are 0.04345 $mg\,mL^{-1}$, 0.04602 $mg\,mL^{-1}$ and 0.05825 $mg\,mL^{-1}$, respectively. The data exhibit that the antitumor activities and IC_{50} of **1** and **2** on SGC7901 cells are similar to the β-Mo_8 cluster with **1** and **2** not exhibiting higher antitumor activities than the parent compound. In contrast, **1** and **2** show different antitumor activities on SMMC7721 cells shown in figure 3, right. Although **1**, **2**, and β-Mo_8 exhibit high antitumor activities on SMMC7721 cells, the inhibitory effects of **1** and **2** are higher than the β-Mo_8 cluster, and the values of IC_{50} for **1**, **2**, and the β-Mo_8 cluster are 0.0643 $mg\,mL^{-1}$, 0.0583 $mg\,mL^{-1}$, and 0.5754 $mg\,mL^{-1}$, respectively. Introduction of Ni-enrofloxacin onto the polyoxoanion surface can modulate antitumor activity, and **1** and **2** possess selective antitumor activities.

Comparing **1** with β-Mo_8, although they are based on the same octamolybdate polyoxoanion, show different antitumor activities. The differences can be reasonably explained by modified chemistry of the POMs. The introduction of Ni-enrofloxacin subunits onto the POMs surface ameliorates the POMs' electronic distribution, polarity, and redox potentials, so that recognition and reactivity of POMs with target biological macromolecules can be altered, resulting in changes of their antitumor activities [5, 10]. Secondly, in the two new compounds, their different antitumor activities may be explained by the differences in their structures. In **1**, Ni-enrofloxacin subunits surround the $\{Mo_8\}$ clusters *via* noncovalent interactions, which result in little effect on the properties of POMs. But Ni-enrofloxacin subunits covalently linking to $\{Mo_8\}$ clusters in **2** may bring a bigger effect on the properties of POMs. Moreover, the configuration of β-Mo_8 cluster is changed into α-Mo_8 isomer. So the distinctive structures lead to the different antitumor activities. Compound **2** exhibits higher antitumor activity than **1**, showing that drug molecules modifying POMs can ameliorate the parent POMs' properties to alter their biological activities. Thus antitumor activity comes from synergism of POMs and enrofloxacin. Finally, **1**, **2**, and β-Mo_8 exhibit different antitumor activities on SGC7901 cell and SMMC7721 cells (figure S7), which indicate that the POMs and their derivatives possess selective antitumor activities.

Combining actual and reported results [10–12], we can draw conclusions that many factors, such as the kinds of POMs and metal ions, the donor characters of ligands, the coordinated environment of POMs, work together to affect antitumor activities, it is difficult to separate and rationalize them. It is also hard to propose definitive reasons why each product generates a different result to our present state of knowledge. So we think that the antitumor activity comes from the synergism of POMs, metal ions, and drug molecules.

4. Conclusion

Two new hybrid compounds were synthesized *via* adjusting the pH of the reaction system, showing that pH plays a key role in control of Mo_8-based hybrids. MTT investigations indicate that these two new compounds possess higher antitumor activities than β-Mo_8 on SMMC7721 cells, which may be due to changes of the properties and configuration of POMs. This work implies that introduction of M-drug onto the octamolybdate surface can ameliorate their antitumor activities. This work provides an example of design and assembly of organic–inorganic hybrid multifunctional materials. Besides enriching the POM family, our work opens opportunities for investigating drugs–TM–POMs systems. These efforts are currently ongoing.

Supplementary material

Crystallographic data and CCDC can be obtained free of charge from the Cambridge Crystallographic Data Centre via www.ccdc.cam.ac.uk/data_request/cif. Tables of selected bond lengths (é), bond angles (degree), and inhibitory effect of compounds on tumor cells in vitro, IR, TG, XRD, and figures for compounds are provided in supporting information.

Acknowledgments

This work is financially supported by the National Natural Science Foundation (Grant No. 20 901 031), the Education Ministry key Teachers Foundation (1155G53), and Scientific and technological project (GC09C317) of Heilongjiang Province.

References

[1] A. Müller, M.T. Pope, F. Peters, D. Gatteschi. *Chem. Rev.*, **98**, 239 (1998).
[2] D.L. Long, R. Tsunashima, L. Cronin. *Angew. Chem. Int. Ed.*, **10**, 1736 (2010).
[3] X.H. Wang, J.F. Liu, M.T. Pope. *Dalton Trans.*, 957 (2003).
[4] J. Li, Y.F. Qi, J. Li. *J. Coord. Chem.*, **57**, 1309 (2004).

[5] J. Li, J. Li, Y.F. Qi, H.F. Wang, E.B. Wang, C.W. Hu, L. Xu, X.Y. Wu. *Chem. J. Chinese Universities*, **6**, 1010 (2004).
[6] W.F. Bu, L.X. Wu, X. Zhang, A.C. Tang. *J. Phys. Chem. B*, **107**, 13425 (2003).
[7] B.L. Moskovitz. *Antimicrob. Agents Chemother.*, **32**, 1300 (1988).
[8] H.Y. An, Z.B. Han, T.Q. Xu. *Inorg. Chem.*, **24**, 11 403 (2010).
[9] S.T. Zheng, J. Zhang, X.X. Li, W.H. Fang, G.Y. Yang. *J. Am. Chem. Soc.*, **132**, 15102 (2010).
[10] J.Q. Sha, L.Y. Liang, X. Li, Y. Zhang, H. Yan, G. Chen. *Polyhedron*, **30**, 1657 (2011).
[11] M. Patel, D. Gandhi, P. Parmar. *J. Coord. Chem.*, **64**, 1276 (2011).
[12] H. Muslu, A. Golcu, M. Tumer, M. Ozsoz. *J. Coord. Chem.*, **64**, 3393 (2011).
[13] I. Turel. *Coord. Chem. Rev.*, **232**, 27 (2002).
[14] P.J. Hagrman, J. Zubieta. *Inorg. Chem.*, **38**, 4480 (1999).
[15] D.G. Allis, E. Burkholder, J. Zubieta. *Polyhedron*, **231**, 145 (2004).
[16] C.D. Wu, C.Z. Lu, H.H. Zhuang, J.S. Huang. *Inorg. Chem.*, **41**, 5636 (2002).
[17] D. Hagrman, P.J. Zapf, J. Zubieta. *Chem. Commun.*, 1283 (1998).
[18] Y.Q. Lan, S.L. Li, X.L. Wang, K.Z. Shao, D.Y. Du, H.Y. Zang, Z.M. Su. *Inorg. Chem.*, **47**, 8179 (2008).
[19] H.Y. Liu, H. Wu, J. Yang, Y.Y. Liu, B. Liu, Y.Y. Liu, J.F. Ma. *Cryst. Growth Des.*, **11**, 2920 (2011).
[20] G.M. Sheldrick. *SHELX-97*, *Program for Crystal Structure Refinement*, University of Göttingen, Germany (1997); G.M. Sheldrick. *SHELXL-97*, *Program for Crystal Structure Solution*, University of Göttingen, Germany (1997).
[21] E.K. Efthimiadou, Y. Sanakis, M. Katsarou, C.P. Raptopoulou, A. Karaliota, N. Katsaros, G. Psomas. *J. Inorg. Biochem.*, **100**, 1378 (2006).
[22] C.J. Zhang, H.J. Pang, Q. Tang, H.Y. Wang, Y.G. Chen. *New J. Chem.*, **35**, 190 (2011).